IEEE Access
Multidisciplinary | Rapid Review | Open Access Journal

Received September 20, 2021, accepted September 30, 2021, date of publication October 4, 2021, date of current version October 11, 2021.

Digital Object Identifier 10.1109/ACCESS.2021.3117448

Current Sensors Offset Fault Online Estimation in Permanent Magnet Synchronous Generator (PMSG) Drives for Offshore Wind Turbines

XIAOGANG DING[1,2], YIXUAN ZHANG[3], AND ZONGBIN YE[1], (Member, IEEE)
[1]School of Electrical and Power Engineering, China University of Mining and Technology, Xuzhou 221116, China
[2]Pushon-Electric Company Ltd., Beijing 100080, China
[3]Department of Electronic Engineering, University of York, York YO10 5DD, U.K.

Corresponding author: Yixuan Zhang (yz4434@york.ac.uk)

This work was supported by the Fundamental Research Funds for the Central Universities under Grant 2019XKQYMS36.

ABSTRACT Offshore wind power generation system's reliability is always a challenging task. To solve the current sensor offset fault problem in the electric powertrain for the offshore wind power generation system, in this paper, a current-detection based sensor offset fault diagnosis method is proposed. The proposed method adopts four fixed measuring points for the estimation of the offset values, which does not require any modifications to the traditional PWM generating strategy. Therefore, the total harmonic distortion (THD) of the drive is not increased by using the proposed offset fault estimation method. The offset fault parameters of the powertrain system are obtained by analyzing the detected current sensors in the aforementioned four sampling points directly. No complex observers nor filters are needed for the signal processing, resulting in computational burden reduction. Experimental results on a 1 kW PMSG system demonstrated the effectiveness of the proposed strategy, which show that the current sensor offset faults can be estimated accurately, and the adverse effects can be eliminated.

INDEX TERMS Current sensor, offset fault, permanent magnet synchronous generator.

I. INTRODUCTION

As a renewable energy source, wind energy has reached 550 GW of cumulative installed power in the world so far and contributes much of the total generation capacity, however, of which only about 20 GW of production share comes from offshore farms [1], [2]. In addition, as a promising topology for offshore wind energy, direct-driven permanent magnet synchronous generators (PMSGs) has been well developed in the past ten years owing to the advantages of gearbox-free structure [2]. PMSGs are extensively used in industrial and household areas because of their higher efficiency, higher power density and better performance compared with induction machines [3]–[7]. To realize the advantages of PMSG drives, the closed-loop control technique is necessary. To achieve this goal, different types of sensors are installed in the drive, such as the rotor position sensor, the voltage sensor, and several current sensors. The faults of any sensor will have a serious impact on the system, and can even lead to system shutdown.

Usually, a three-phase PMSG drive are equipped with one DC link and three-phase current sensors [8]–[10]. The offset faults of the phase-current sensors will degrade the system performance and even lead to system shutdown [11]–[21]. To be specific, the offset faults of the phase current sensors will introduce torque ripples with the fundamental operation frequency, which might a significant increase in harmful vibration of the system and thus eventually affecting the operating lifespan period. Therefore, it is necessary to diagnose and estimate the offset faults of current sensors.

To solve the related technical problem, researchers have presented many different solutions. In [2], the low-voltage ride-through problem during grid faults are investigated including the overvoltage suppression and the design of active power limitation.

Among all current sensor offset fault estimation methods, the observer based schemes and the system variable analysis based scheme are the more mainstream strategies.

The associate editor coordinating the review of this manuscript and approving it for publication was Grigore Stamatescu.

Literature [11] proposed a torque ripple decline strategy to eliminate current offset faults, which is irrelevant to the motor parameters. The current offset fault is deduced from the output voltage and/or the feedback current signals. By selecting the appropriate estimation method, the time required for the diagnosis process can be greatly reduced. In [12], [13], the current offset and scaling faults are compensated using the reference voltage signals, which can be applied in all operation applications in motor drives. The current signal missing faults is investigated in [14], which takes full advantage of the current amplitude information and is independent of the precise model parameters. In [15], a current and position sensor fault diagnosis method is proposed, which considers the parameter and load fluctuations. A sliding-mode observer based current measurement faults estimation method is proposed regarding the sensorless controlled motor drive in [20]. The current ripples elimination method is studied in [21] regarding the current measurement errors. For the torque ripples elimination and motor performance improvements, in [22] the offset faults for current sensors are investigated using the phase voltage commands. By low passing the current commands in motor drives, the current measurement errors can be obtained, which afterwards eliminates the torque ripples [23]. In [24], a current sensor fault diagnosis method is proposed in linear motor systems for subway applications, where both the gain and offset faults can be estimated by comparisons between the estimated and the measured synchronous currents. A periodic disturbance observer is proposed in [25] for the elimination of current sampling faults. The power supply quality for current sensors is investigated in [26] regarding the current sampling offset faults. By analyzing the reference voltage, the current offset fault is compensated in [27]. The offline scaling errors estimation method is investigated in [28], which is not limited by whether the rotor is locked or not. However, this method can only be used in the initial status estimation. However, these methods require complex observers or digital filters for the estimation of the offset faults of phase current sensors, which will introduce additional computational burden to the system. Also, the load type and disturbance might decrease the estimation accuracy of these kinds of methods according to [29].

To solve these drawbacks, the observer and digital free methods are researched in [29], [30]. In [30], a mutual correction approach that utilizes the current sampling information for the current sensors in motor drives is proposed. The advantages are that only two voltage injection points are required, and the mutual correction approach does not affect the normal operation of the drive. In addition, the motor parameters are not necessary for the proposed strategy. However, the proposed strategy needs to change the PWM generating method in the voltage injection points into the proposed asymmetrical type. To solve this limitation, a self-estimation method without using observers and digital filters for phase current sensors faults is proposed in [29], where no additional hardware support is needed. Also, the estimation time can be controlled within 1 ms. However, modifications on the installation methods of phase current sensors are required, which might limit its application.

TABLE 1. Comparison between proposed strategy and existing technologies.

	Anti Disturbance	Do Not Modify PWM or Topology	Online Estimation	Algorithm Simplicity	Estimation Period
System Variable Based Schemes [15, 25]	No	Yes	Yes	No	Several Tens of Seconds
Observer Based Schemes [11-13, 22, 23]	No	Yes	Yes	No	Several Tens of Seconds
Offline Estimation Method [30]	No	Yes	No	Yes	Several Tens of Seconds
Voltage Injection Based Methods [28]	Yes	Yes	Yes	Yes	Several Milliseconds
Topology Modification Based Methods [29]	Yes	No	Yes	Yes	Several Milliseconds
Proposed Strategy	Yes	Yes	Yes	Yes	Several Milliseconds

Current methods mainly employ the output voltages or feedback current information to estimate the current sampling faults, which might increase computational burden owing to the adoption of complex observers and filters. Another problem caused by these methods is the long estimation period, which lasts from tens of seconds to several minutes. The test voltage injection method and related techniques can avoid above problems. However, modifications on the PWM generating method or the topology are required, which also limits its application. Therefore, for solving the aforementioned problems, in this paper, a current-detection based sensor offset fault diagnosis method is proposed. The proposed strategy does not modify the topology nor the PWM generating method of the drive. Only current signals at a few fixed sampling points are needed. Moreover, the estimation process only requires a few multiplications and additional operations. Therefore, the computational burden of the proposed approach is not increased, and the estimation time is controlled within one electrical angle period, which is usually about several milliseconds. The comparison between the proposed strategy and existing technologies are presented in Table 1.

The remainder parts of this paper are structured as below. In section II, the mathematical model of the system considering offset faults is studied. In section III, the proposed estima-

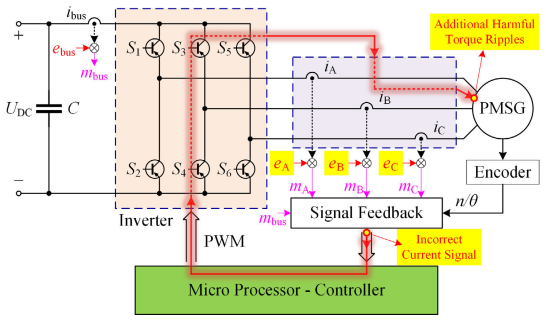

FIGURE 1. PMSG drive considering current offset faults.

tion strategy is illustrated. The overall control approach and experiment results are provided in section IV and section V, respectively. The conclusion is finally drawn in section VI.

II. MATHEMATICAL MODEL CONSIDERING OFFSET FAULTS

The PMSG drive considering current offset faults is illustrated in Figure 1. The inverter is supplied by the DC-bus capacitor C with voltage of U_{DC}. $S_1,\ldots,S_6$ are the six power devices of the two-level inverter. The current sensors measure the three-phase currents i_A, i_B, i_C and the DC-bus current i_{bus}. The rotor position is measured by the encoder and the PWM signals are generated by the controller - a microprocessor.

In Figure 1, the offset faults of the sampling circuits are considered within the circuit, where e_A, e_B, e_C, e_{bus} and m_A, m_B, m_C, m_{bus} are the offset values and the measured currents which can be expressed in (1):

$$\begin{cases} m_A = i_A + e_A \\ m_B = i_B + e_B \\ m_C = i_C + e_C \\ m_{bus} = i_{bus} + e_{bus} \end{cases} \tag{1}$$

It can be seen from figure 1 that the offset faults of phase current sensors are introduced to the controller through the sampling circuits. And then, the control sends out the switching signals containing inaccurate information to the inverter. Finally, the inverter drives the motor in an incorrect manner, which results in extra harmful torque ripples.

In this paper, the relations among all the current sensors are taken full advantage of for the estimation of the phase current sensor offset faults. According to the topology of the inverter, the switching state of the inverter is relevant to the relations among these measured currents [31], which are illustrated in Table 2. It can be observed from Table 2 that the offset faults of the current sampling circuits can be deduced by the measured currents in specific sampling points directly.

III. PROPOSED ESTIMATION METHOD

A. ESTIMATION OF OFFSET FAULT FOR DC-BUS CURRENT SENSOR

It can be investigated from Table 2 that the DC-bus current sensor offset is equal to the measured DC-bus current in

TABLE 2. The relations among the measured currents.

Switching States	S_{000}	S_{100}	S_{110}	S_{010}
m_{bus}	e_{bus}	$i_A + e_{bus}$	$-i_C + e_{bus}$	$i_B + e_{bus}$
m_A	$i_A + e_A$	$i_A + e_A$	$i_A + e_A$	$i_A + e_A$
m_B	$i_B + e_B$	$i_B + e_B$	$i_B + e_B$	$i_B + e_B$
m_C	$i_C + e_C$	$i_C + e_C$	$i_C + e_C$	$i_C + e_C$
Switching States	S_{011}	S_{001}	S_{101}	S_{111}
m_{bus}	$-i_A + e_{bus}$	$i_C + e_{bus}$	$-i_B + e_{bus}$	e_{bus}
m_A	$i_A + e_A$	$i_A + e_A$	$i_A + e_A$	$i_A + e_A$
m_B	$i_B + e_B$	$i_B + e_B$	$i_B + e_B$	$i_B + e_B$
m_C	$i_C + e_C$	$i_C + e_C$	$i_C + e_C$	$i_C + e_C$

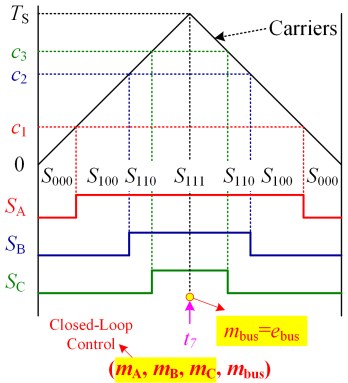

FIGURE 2. Traditional SVPWM waveform (Section I).

switching states of the zero vectors V_{000} and V_{111}. In Figure 2, the conventional seven-segment space vector pulse width modulation (SVPWM) waveform in Section I is illustrated, where c_1, c_2 and c_3 are three comparators and S_A, S_B and S_C are the operating status of the three-phase bridge arms. The feedback current information for closed-loop control, i.e., m_A, m_B and m_C are sampled at the middle of each PWM cycle. From Figure 2, it can be seen that at the intermediate point of each PWM period, t_7, the switching states of the inverter is always S_{111}. Therefore, by sampling the DC-bus current value at t_7, the offset fault of the DC-bus current sensor can be estimated with (2),

$$e_{bus} = m_{bus}[t_7], \tag{2}$$

where $m_{bus}[t_7]$ is the measured DC-bus current value at sampling point t_7.

B. ESTIMATION OF OFFSET FAULT FOR THREE-PHASE CURRENT SENSORS

It can be observed from Table 2 that the offset faults of the three-phase current sensors are related to the DC-bus current sampling values based on the operating conditions of the inverter. In this part, the estimation of the offset faults of the three-phase current sensors is analyzed in detail.

1) ESTIMATION OF e_A

In Table 2, the current relations among m_{bus} and m_{A} under switching states of S_{100} is given in (3):

$$\begin{cases} m_{bus}\left[S_{100}\right] = i_A\left[S_{100}\right] + e_{bus} \\ m_A\left[S_{100}\right] = i_A\left[S_{100}\right] + e_A, \end{cases} \tag{3}$$

where $i_{\text{A}}[S_{100}]$ denotes the actual phase-A current value under switching states of S_{100}; $m_{\text{bus}}[S_{100}]$ and $m_{\text{A}}[S_{100}]$ are the measured phase-A and DC bus current values under switching states of S_{100}.

Thus, the offset error of phase-A current sensor is able to be deduced as given in (4):

$$e_A = m_A\left[S_{100}\right] - m_{bus}\left[S_{100}\right] + e_{bus}. \tag{4}$$

2) ESTIMATION OF e_B

In Table 2, the current relations among m_{bus} and m_{B} under switching states of S_{010} is given in (5):

$$\begin{cases} m_{bus}\left[S_{010}\right] = i_B\left[S_{010}\right] + e_{bus} \\ m_B\left[S_{010}\right] = i_B\left[S_{010}\right] + e_B, \end{cases} \tag{5}$$

where $i_{\text{B}}[S_{010}]$ denotes the actual phase-B current value under switching states of S_{010}; $m_{\text{bus}}[S_{010}]$ and $m_{\text{B}}[S_{010}]$ are the measured DC-bus and phase-B current values under switching states of S_{010}.

Thus, the offset error of phase-B current sensor is able to be deduced as given in (6):

$$e_B = m_B\left[S_{010}\right] - m_{bus}\left[S_{010}\right] + e_{bus}. \tag{6}$$

3) ESTIMATION OF e_C

In Table 2, the current relations among m_{bus} and m_{C} under switching states of S_{001} is given in (7):

$$\begin{cases} m_{bus}\left[S_{001}\right] = i_C\left[S_{001}\right] + e_{bus} \\ m_C\left[S_{001}\right] = i_C\left[S_{001}\right] + e_C, \end{cases} \tag{7}$$

where $i_C[S_{001}]$ denotes the actual phase-C current value under switching states of S_{001}; $m_{\text{bus}}[S_{001}]$ and $m_{\text{C}}[S_{001}]$ are the measured DC-bus and phase-C current values under switching states of S_{001}.

Thus, the offset error of phase-C current sensor is able to be deduced as given in (8):

$$e_C = m_C\left[S_{001}\right] - m_{bus}\left[S_{001}\right] + e_{bus}, \tag{8}$$

4) FIXED CURRENT SAMPLING POINTS

From parts 1, 2, and 3, the estimation algorithm for the three-phase current sensors is illustrated. However, the required currents signals must be sampled under specific switching states. Therefore, in this part, the fixed current sampling points for the acquisition of these crucial signals will be explained.

In Figure 2, it can be observed that the operation time of each active voltage vector is determined by the three comparators of c_1, c_2 and c_3. Specifically, the operation time for both the zero and active vectors are determined by c_1 and c_3 as given in (9):

$$\begin{cases} T_{zero} = T_S - c_3 + c_1 = 2c_1 \\ T_{active} = T_S - T_{zero} = T_S - 2c_1, \end{cases} \tag{9}$$

where T_{zero} and T_{active} denote the operation time of the zero and active vectors, respectively; T_{S} is the switching period of the inverter.

In this paper, the settled sampling points is designed at a quarter of the PWM cycle. To be specific, sampling points t_1, t_3 and t_5 are designed to be located under switching states of S_{100}, S_{010} and S_{001}, respectively. To acquire an accurate current sampling value, the action period of each switching state should be long enough. Also, the sampling points should not be located near the edge of the corresponding switching period. As a result, the rules for the values of the three comparators are:

i. The acting time for the active vectors should be longer than the zero vectors.

ii. The acting time for the switching state corresponding to the sampling point should hold the most acting time of the active vectors.

These rules can be explained in (10) to (12):

$$\text{For} S_{100}(t_1): \begin{cases} c_1 < \dfrac{T_S}{4} \\ |c_3 - c_2| < t_{min}, \end{cases} \tag{10}$$

where t_{min} denotes the required action time for the active vector not for current sampling.

$$\text{For} S_{010}(t_3): \begin{cases} c_2 < \dfrac{T_S}{4} \\ |c_1 - c_3| < t_{min}, \end{cases} \tag{11}$$

$$\text{For} S_{001}(t_5): \begin{cases} c_3 < \dfrac{T_S}{4} \\ |c_2 - c_1| < t_{min}, \end{cases} \tag{12}$$

It is obvious that:

i. At the high modulation areas, the acting time of the zero vectors complies with rule No. 1.

ii. At each boundary of the six sectors, the acting time for the corresponding active vectors meets the aforementioned rule No. 2.

Therefore, the three fixed current sampling points are exhibited in Figure 3. It can be observed that the three current sampling points are positioned at the corresponding sector boundaries. And the aforementioned rules can be satisfied.

IV. OVERALL CONTROL STRATEGY

A. SAMPLING POINTS FOR ESTIMATION OF CURRENT OFFSET FAULTS

From the previous contents, it can be observed that the four fixed sampling points, t_1, t_3, t_5 and t_7 can be measured within one electrical angle cycle. It can be observed that the sampling point t_7 should not be measured at the high modulation area. Therefore, to achieve a fast estimation period requirement, the appropriate estimation process should be located

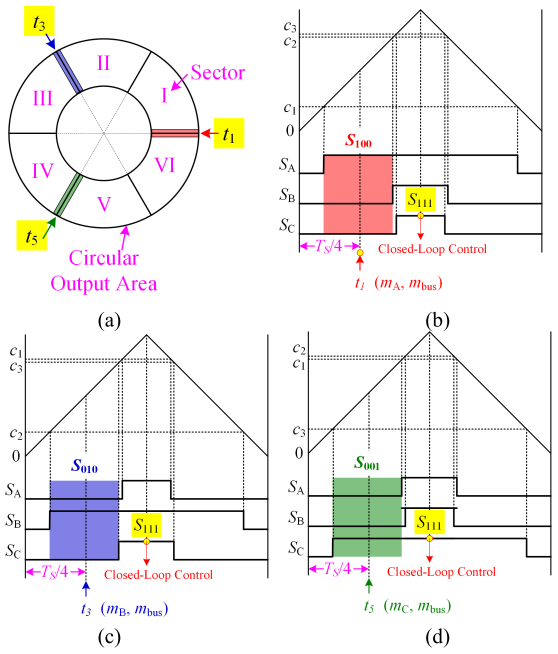

FIGURE 3. Three fixed current sampling points: (a) Location of three fixed sampling points; (b) PWM waveform of sampling point t_1; (c) PWM waveform of sampling point t_3; (d) PWM waveform of sampling point t_5.

at the middle modulation area. As a result, the acting time requirements for all four sampling points can be satisfied.

B. SAMPLING POINTS FOR CLOSED-LOOP CONTROL

Because the three-phase currents are measured by the corresponding current sensors, the sampling points for the closed-loop control can be placed at any time. However, for the convenience of easy implementation, in this article, the sampling points for the closed-loop control is designed at the middle point of each PWM control period. To be specific:

i. During normal operation periods where the four fixed sampling points are not required, the fixed sampling point is located at the intermediate point of the corresponding PWM period. At this condition, only the three-phase currents will be sampled for the closed-loop control, which is illustrated in figure 2;

ii. During estimation periods where only the t_7 is required, the fixed sampling point is located at the intermediate point of the corresponding PWM period. At this condition, all the four current sensors measure the corresponding current, where the three-phase currents are utilized for the closed-loop control whereas the DC-bus current is used for the estimation of e_{bus};

iii. During estimation periods where any of the other three fixed sampling points is required, two sampling points are positioned at the quarter and the intermediate point of the PWM period, respectively. At this condition, the DC-bus current sensor and the corresponding phase current sensor measure the currents at the quarter of the PWM cycle for the estimation of offset faults. At the intermediate point of the PWM period, all the three-phase current sensors measure the corresponding currents for the closed-loop control.

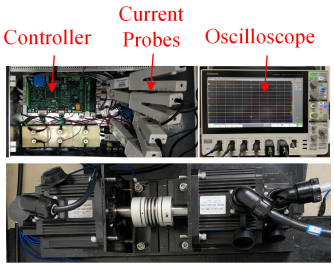

FIGURE 4. Experiment setup.

TABLE 3. Parameters of motor prototype and offset faults.

Parameters	Value	Parameters	Value
Rated Power	1 kW	Rated Voltage	100 V
Rated Current	7 A	Line Resistance	1 Ω
Line Inductance	2.3 mH	Rotor Inertia	$1*10^{-3}$ kg.m^2
Rated Speed	2000 rpm	Rated Torque	5 N.m
e_A	0.5 A	e_B	0.7 A
e_C	-0.4 A	e_{bus}	-0.5 A

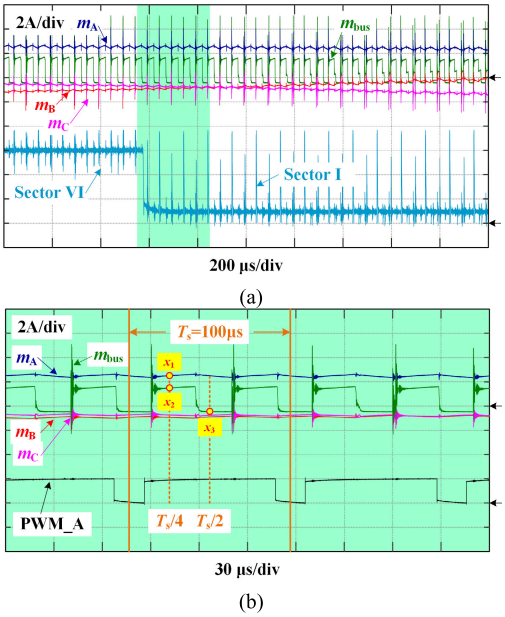

FIGURE 5. Experiment results at t_1: (a) Currents and Sector signal waveform; (b) Zoom in view of (a).

V. EXPERIMENT RESULTS

For verifying the effectiveness of the proposed strategy, the experiment is implemented on a 1-kW PMSG prototype. The experimental setup is illustrated in Figure 4. The control unit is a digital signal processor TMS320F2812. The current sensors installed in the drive are hall-effect sensors, LEM, LT58/S7. The inverter is an intelligent power module, Mitsubishi, PM75RL1A120. The current probes are used for signal observation. The parameters of the offset faults and the motor are given in Table 3.

In Figure 5, the experiment result at sampling point t_1 is presented. During the sector boundary between sector VI and sector I, the output voltage vector has almost the same phase angle as the basic voltage vector V_1 as can be seen in figure 3(a). Therefore, the action time of V_1 is much longer than

TABLE 4. Measured currents.

Sampling Period	Sampling Point	Parameters	Value
Sector Boundary	t_1	$m_A[S_{100}]$ (x_1)	2.51 A
Between Sectors		$m_{bus}[S_{100}]$ (x_2)	1.49 A
VI and I (Figure 4)	t_7	$m_{bus}[S_{111}]$ (x_3)	-0.47 A
Sector Boundary	t_3	$m_B[S_{010}]$ (x_4)	2.45 A
Between Sectors		$m_{bus}[S_{010}]$ (x_5)	1.21 A
II and III (Figure 5)	t_7	$m_{bus}[S_{111}]$ (x_6)	-0.46 A
Sector Boundary	t_5	$m_C[S_{001}]$ (x_7)	1.69 A
Between Sectors		$m_{bus}[S_{001}]$ (x_8)	1.58 A
IV and V (Figure 6)	t_7	$m_{bus}[S_{111}]$ (x_9)	-0.47 A

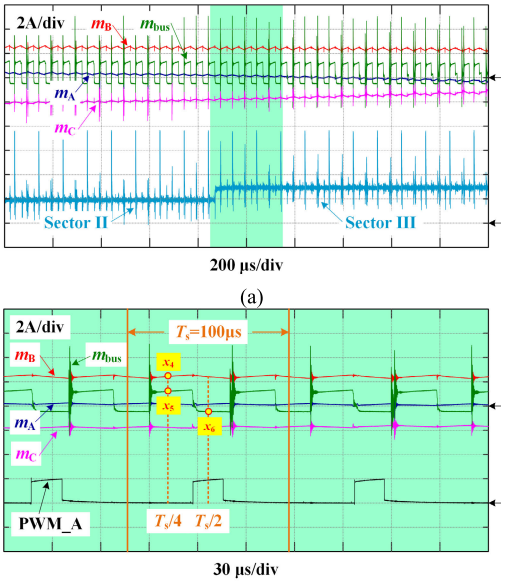

FIGURE 6. Experiment results at t_3: (a) Currents and Sector signal waveform; (b) Zoom in view of (a).

that of the basic vector V_2 as can be seen from figure 3(b). In the PWM cycle corresponding to sampling point t_1, there exist two fixed current sampling points. The first sampling point is located at the $T_S/4$ of the PWM cycle, which measures the phase-A current $m_A[S_{100}]$ (x_1 in figure 5 (b)) and the DC-bus current $m_{bus}[S_{100}]$ (x_2 in figure 5(b)). The second sampling point is located at the $T_S/2$ of the PWM cycle, which measures all the current values, of which the phase current values are directly used for the closed-loop control, whereas the DC-bus one, $m_{bus}[S_{111}]$ (x_3 in figure 5(b)) is used for parameter estimation. The measured currents are presented in Table 4.

In Figure 6, the experiment result at sampling point t_3 is presented. During the sector boundary between sector II and sector III, the output voltage vector has almost the same phase angle as the basic voltage vector V_3 as can be seen in figure 3(a). Therefore, the action time of V_3 is much longer than that of the basic vector V_4 as can be seen from figure 3(c). In the PWM cycle corresponding to sampling point t_3, there exist two fixed current sampling points. The first sampling point is located at the $T_S/4$ of the PWM cycle, which measures the phase-B current $m_B[S_{010}]$ (x_4 in figure 6 (b)) and the

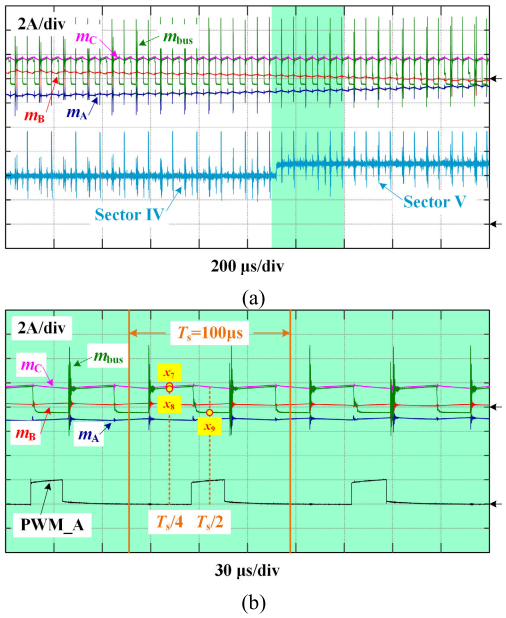

FIGURE 7. Experiment results at t_5 (a) Currents and Sector signal waveform; (b) Zoom in view of (a).

TABLE 5. Estimated current offset faults.

Parameters	Value	Error	Parameters	Value	Error
e_A	0.55 A	0.05 A	e_B	0.77 A	0.07 A
e_C	-0.36 A	0.04 A	e_{bus}	-0.47 A	0.03 A

DC-bus current $m_{bus}[S_{010}]$ (x_5 in figure 6 (b)). The second sampling point is located at the $T_S/2$ of the PWM cycle, which measures all the current values, of which the phase current values are directly used for the closed-loop control, whereas the DC-bus one, $m_{bus}[S_{111}]$ (x_6 in figure 6 (b)) is used for parameter estimation. The measured currents are presented in Table 4.

In Figure 7, the experiment result at sampling point t_5 is presented. During the sector boundary between sector IV and sector V, the output voltage vector has almost the same phase angle as the basic voltage vector V_5 as can be seen in figure 3(a). Therefore, the action time of V_5 is much longer than that of the basic vector V_6 as can be seen from figure 3(d). In the PWM cycle corresponding to sampling point t_5, there exist two fixed current sampling points. The first sampling point is located at the $T_S/4$ of the PWM cycle, which measures the phase-C current $m_C[S_{001}]$ (x_7 in figure 7(b)) and the DC-bus current $m_{bus}[S_{001}]$ (x_8 in figure 7(b)). The second sampling point is located at the $T_S/2$ of the PWM cycle, which measures all the current values, of which the phase current values are directly used for the closed-loop control, whereas the DC-bus one, $m_{bus}[S_{111}]$ (x_9 in figure 7 (b)) is used for parameter estimation. The measured currents are presented in Table 4.

By using the experimental data in Table 4, the offset fault of the DC-bus current sensor can be obtained in (13).

$$e_{bus} = (x_3 + x_6 + x_9)/3 \approx -0.47\text{A}, \tag{13}$$

The offset fault of the phase-A current sensor can be obtained in (14).

$$e_A = x_1 - x_2 + e_{bus} \approx 0.55\text{A}, \tag{14}$$

The offset fault of the phase-B current sensor can be obtained in (15).

$$e_A = x_4 - x_5 + e_{bus} \approx 0.77\text{A}, \tag{15}$$

The offset fault of the phase-C current sensor can be obtained in (16).

$$e_A = x_7 - x_8 + e_{bus} \approx -0.36\text{A}, \tag{16}$$

Therefore, the estimated current offset faults can be deduced from the experimental results, which are presented in Table 5. Compared with the actual current offset faults, the estimated values have little estimation error, which prove the effectiveness of the proposed method.

VI. CONCLUSION

In this paper, a current-detection based current sensor offset fault estimation method for PMSG drives is proposed, which makes the best use of the relations among all the available sensor information. Compared with the existing techniques, the proposed strategy does not rely on the observers or filters, resulting in a decreased computational burden. Also, the proposed strategy does not modify the PWM generating method nor the installation methods of the phase current sensors. Therefore, the proposed strategy is easy to implement. The proposed method is examined by an experiment on a 1 kW motor, which shows that the offset faults is able to be estimated accurately. The advantages of the proposed strategy are:

1) The proposed strategy only needs a few multiplication and addition operations, which greatly reduce the computational burden of the controller.

2) Because the estimation time is controlled to be shorter than one electrical angle period, which is usually about several milliseconds, the required estimation period is short.

3) There is no need to modify the control algorithm, the PWM generation method and the topology of the inverter. Therefore, the proposed strategy is easier to implement.

REFERENCES

[1] M. A. Gonzalez-Cagigal, J. A. Rosendo-Macias, and A. Gomez-Exposito, "Parameter estimation of wind turbines with PMSM using cubature Kalman filters," *IEEE Trans. Power Syst.*, vol. 35, no. 3, pp. 1796–1804, May 2020.

[2] M. Nasiri and R. Mohammadi, "Peak current limitation for grid side inverter by limited active power in PMSG-based wind turbines during different grid faults," *IEEE Trans. Sustain. Energy*, vol. 8, no. 1, pp. 3–12, Jan. 2017.

[3] M. Wang, D. Sun, W. Ke, and H. Nian, "A universal lookup table-based direct torque control for OW-PMSM drives," *IEEE Trans. Power Electron.*, vol. 36, no. 6, pp. 6188–6191, Jun. 2021.

[4] C. Xia, S. Wang, X. Gu, Y. Yan, and T. Shi, "Direct torque control for VSI-PMSM using vector evaluation factor table," *IEEE Trans. Ind. Electron.*, vol. 63, no. 7, pp. 4571–4583, Jul. 2016.

[5] Y. Xiao, C. Liu, and F. Yu, "An integrated on-board EV charger with safe charging operation for three-phase IPM motor," *IEEE Trans. Ind. Electron.*, vol. 66, no. 10, pp. 7551–7560, Oct. 2019.

[6] J. Lu, Y. Hu, J. Liu, and Z. Wang, "All current sensor survivable IPMSM drive with reconfigurable inverter," *IEEE Trans. Ind. Electron.*, vol. 67, no. 8, pp. 6331–6341, Aug. 2020.

[7] Y. Xiao and C. Liu, "A study of rotational movement and charging torque of reconfigured on-board charger," *IEEE Trans. Power Electron.*, vol. 35, no. 10, pp. 10720–10728, Oct. 2020.

[8] Z. Wang, J. Chen, M. Cheng, and K. T. Chau, "Field-oriented control and direct torque control for paralleled VSIs fed PMSM drives with variable switching frequencies," *IEEE Trans. Power Electron.*, vol. 31, no. 3, pp. 2417–2428, Mar. 2016.

[9] C. Gong, Y. Hu, J. Gao, Z. Wu, J. Liu, H. Wen, and Z. Wang, "Winding-based DC-bus capacitor discharge technique selection principles based on parametric analysis for EV-PMSM drives in post-crash conditions," *IEEE Trans. Power Electron.*, vol. 36, no. 3, pp. 3551–3562, Mar. 2021.

[10] J. Lara, J. Xu, and A. Chandra, "Effects of rotor position error in the performance of field-oriented-controlled PMSM drives for electric vehicle traction applications," *IEEE Trans. Ind. Electron.*, vol. 63, no. 8, pp. 4738–4751, Aug. 2016.

[11] K. Nishizawa, J.-I. Itoh, and Y. Nishizawa, "Quick compensation method of motor phase current sensor offsets without motor parameters for PMSM drive," in *Proc. IEEE Energy Convers. Congr. Expo. (ECCE)*, Oct. 2017, pp. 5877–5883.

[12] M. Kim, S.-K. Sul, and J. Lee, "Compensation of current measurement error for current-controlled PMSM drives," in *Proc. IEEE Energy Convers. Congr. Expo. (ECCE)*, Sep. 2012, pp. 487–494.

[13] M. Kim, S.-K. Sul, and J. Lee, "Compensation of current measurement error for current-controlled PMSM drives," *IEEE Trans. Ind. Appl.*, vol. 50, no. 5, pp. 3365–3373, Sep. 2014.

[14] C. Wu, C. Guo, Z. Xie, F. Ni, and H. Liu, "A signal-based fault detection and tolerance control method of current sensor for PMSM drive," *IEEE Trans. Ind. Electron.*, vol. 65, no. 12, pp. 9646–9657, Dec. 2018.

[15] K. Choi, Y. Kim, S.-K. Kim, and K.-S. Kim, "Current and position sensor fault diagnosis algorithm for PMSM drives based on robust state observer," *IEEE Trans. Ind. Electron.*, vol. 68, no. 6, pp. 5227–5236, Jun. 2021.

[16] M. E. Haque, S. M. Chowdhury, O. Gundogmus, A. Chowdhury, Y. Sozer, F. Venegas, and D. Colavincenzo, "Modeling and analysis of sensor error effects on DC-link current ripple in switched reluctance machine drives," in *Proc. IEEE Energy Convers. Congr. Expo. (ECCE)*, Oct. 2020, pp. 2995–3001.

[17] W.-S. Im, S.-H. Hwang, J.-M. Kim, and J. Choi, "Analysis and compensation of current measurement errors in a doubly fed induction generator," in *Proc. IEEE Energy Convers. Congr. Expo.*, Sep. 2009, pp. 1713–1719.

[18] T. Q. Nam, C. F. Hoong, T. Yi, and W. Peng, "A control strategy to compensate for current and voltage measurement errors in three-phase PWM rectifiers," in *Proc. IEEE Energy Convers. Congr. Expo. (ECCE)*, Oct. 2017, pp. 4601–4608.

[19] S. Cheng, D. Wang, and J. Chen, "Current measurement gain tuning for interior permanent magnet synchronous motor (IPMSM) drives using controlled short circuit tests," in *Proc. IEEE Conf. Expo Transp. Electrific. Asia–Pacific (ITEC Asia–Pacific)*, Aug. 2014, pp. 1–6.

[20] S. Ye and X. Yao, "An enhanced SMO-based permanent-magnet synchronous machine sensorless drive scheme with current measurement error compensation," *IEEE J. Emerg. Sel. Topics Power Electron.*, vol. 9, no. 4, pp. 4407–4419, Aug. 2021.

[21] C.-N. Heo, S.-H. Hwang, and D.-J. Bang, "Current ripple reduction due to current measurement errors of independent three-phase permanent magnet synchronous machine with dual air-gap," in *Proc. IEEE 2nd Int. Future Energy Electron. Conf. (IFEEC)*, Nov. 2015, pp. 1–6.

[22] H. Tamura, J.-I. Itoh, and Y. Noto, "Two methods for compensating motor-current-sensor offset error by using DC-voltage component included in phase-voltage command for current-controlled PMSM drive," in *Proc. 17th Eur. Conf. Power Electron. Appl. (EPE ECCE-Eur.)*, Sep. 2015, pp. 1–10.

[23] K.-W. Lee and S.-I. Kim, "Dynamic performance improvement of a current offset error compensator in current vector-controlled SPMSM drives," *IEEE Trans. Ind. Electron.*, vol. 66, no. 9, pp. 6727–6736, Sep. 2019.

[24] W. Wang, W. Tian, Z. Wang, W. Hua, and M. Cheng, "A fault diagnosis method for current sensors of primary permanent-magnet linear motor drives," *IEEE Trans. Power Electron.*, vol. 36, no. 2, pp. 2334–2345, Feb. 2021.

[25] T. Yamaguchi, Y. Tadano, and N. Hoshi, "Compensation of the current measurement error with periodic disturbance observer for motor drive," in *Proc. Int. Power Electron. Conf. (IPEC-Hiroshima–ECCE ASIA)*, May 2014, pp. 1242–1246.

[26] C. Liu and H. J.-G. Liu, "Offset error reduction in open loop Hall effect current sensors powered with single voltage source," in *Proc. IEEE Int. Workshop Appl. Meas. Power Syst. (AMPS)*, Sep. 2014, pp. 1–6.
[27] H. Tamura, T. Ajima, and Y. Noto, "A torque ripple reduction method by current sensor offset error compensation," in *Proc. 15th Eur. Conf. Power Electron. Appl. (EPE)*, Sep. 2013, pp. 1–10.
[28] M.-S. Yoo, S.-W. Park, H.-J. Lee, and Y.-D. Yoon, "Offline compensation method for current scaling gains in AC motor drive systems with three-phase current sensors," *IEEE Trans. Ind. Electron.*, vol. 68, no. 6, pp. 4760–4768, Jun. 2021.
[29] J. Lu, Y. Hu, J. Liu, and H. Wen, "Self-calibration of phase current sensors with sampling errors by multipoint sampling of current values in a single PWM cycle," *IEEE Trans. Ind. Electron.*, vol. 68, no. 4, pp. 2942–2951, Apr. 2021.
[30] J. Lu, Y. Hu, G. Chen, Z. Wang, and J. Liu, "Mutual calibration of multiple current sensors with accuracy uncertainties in IPMSM drives for electric vehicles," *IEEE Trans. Ind. Electron.*, vol. 67, no. 1, pp. 69–79, Jan. 2020.
[31] H. Lu, X. Cheng, W. Qu, S. Sheng, Y. Li, and Z. Wang, "A three-phase current reconstruction technique using single DC current sensor based on TSPWM," *IEEE Trans. Power Electron.*, vol. 29, no. 3, pp. 1542–1550, Mar. 2014.

XIAOGANG DING received the master's degree in electrical engineering from the School of Information and Electrical Engineering, China University of Mining and Technology, Xuzhou, China, in 2012.

Since 2015, he has been working as the Research Director at Pushon-Electric Company Ltd., Beijing, China. He has authored over ten journal articles and conference papers. His research interests include inverter control and motor drives.

YIXUAN ZHANG received the bachelor's and master's degrees in electrical engineering from the University of Liverpool, U.K., in 2017 and 2018, respectively. He is currently pursuing the Ph.D. degree with the University of York, U.K.

His research interests include integrated power and signal transmission, battery management systems, and power converters.

ZONGBIN YE (Member, IEEE) was born in Jiangxi, China, in 1983. He received the Ph.D. degree in electrical engineering from China University of Mining and Technology, China, in 2010. Since 2015, he has been an Associate Professor with the School of Information and Electrical Engineering, China University of Mining and Technology. He is engaged in research and development of high-power multilevel converters and motor drivers. He has authored many journal articles and conference papers and also one book in the areas of motor control area.